Electronic eye for the prediction of parameters related to grape ripening

G. Orlandi[1], R. Calvini[1,2], L. Pigani[2,3], G. Foca[1,2], G. Vasile Simone[3], A. Antonelli[1,2], A. Ulrici[1,2*]

[1] Dipartimento di Scienze della Vita, Università di Modena e Reggio Emilia, Padiglione Besta, Via Amendola, 2 – 42122 Reggio Emilia
[2] Centro Interdipartimentale BIOGEST-SITEIA, Università degli Studi di Modena e Reggio Emilia, Piazzale Europa, 1 – 42122 Reggio Emilia
[3] Dipartimento di Scienze Chimiche e Geologiche, Università degli Studi di Modena e Reggio Emilia, Via G. Campi, 103 – 41125 Modena
*alessandro.ulrici@unimore.it

Abstract

An electronic eye (EE) for fast and easy evaluation of grape phenolic ripening has been developed. For this purpose, berries of different grape varieties were collected at different harvest times from veraison to maturity, then an amount of the derived must was deposited on a white sheet of absorbent paper to obtain a sort of paper chromatography. Thus, RGB images of the must spots were collected using a flatbed scanner and converted into one-dimensional signals, named *colourgrams*, which codify the colour properties of the images. The dataset of colourgrams was used to build calibration models to relate the colour of the images with the phenolic composition of the samples – determined by reference analytical methods – and therefore to follow the ripening trend. Satisfactory calibration models were obtained for the prediction of the most important parameters related to phenolic ripening of grapes, such as colour index, tonality, total anthocyanins content, malvidin-3-O-glucoside and petunidin-3-O-glucoside.

Keywords

Optical sensors; Image analysis; Multivariate calibration; Phenolic ripening; Grapes; Anthocyanins.

1 Introduction

The maturity level of grapes (*Vitis Vinifera*) at the harvest is the first factor that influences the quality of the resulting wine [1]. Among the various features, sugar content, pH and acidity levels are the parameters more frequently used to monitor the maturity level of grapes [2]. However, also the phenolic composition of grapes plays an important role on the development of several sensorial attributes of wine, such as colour, body, structure, bitterness and astringency [3].

The determination of the parameters related to phenolic ripening is performed by means of classical analytical procedures, mainly based on UV-Vis spectrophotometry and high-performance liquid chromatography [4-6]. These methods are very accurate but require expensive instrumentations and the involvement of skilled personnel. Alternatively, sensory analysis is frequently used to provide a description of colour, aroma, flavour and texture of the grapes, giving a global characterisation of the maturity level [7]. However, the sensory evaluation requires a lot of training and experience to minimize the inherent subjectivity and the variability of tasters [8].

For these reasons, nowadays increased efforts are devoted to develop easy-to-use, inexpensive and objective methods based on artificial sensors [9], known as electronic nose (EN) [10, 11], electronic tongue (ET) [12, 13] and electronic eye (EE) [14, 15]. These devices are generally used to analyse the sample 'as it is' or after a minimal manipulation. Then, the sensor output is processed by proper chemometric techniques that, following a blind-analysis approach, extract the sought information, such as the amount of specific analytes or the sensory features responsible of smell, taste and colour of the sample.

In a recently published paper, some of us have presented an ET aimed at monitoring grape ripening [16]. In that work it was shown that, by proper fusion of the data measured with two voltammetric sensors, it was possible to quantify the parameters related to the technological maturity of grapes, i.e., pH, total acidity and sugar content, in addition to the anthocyanins content. In the present work, which was conducted on the same grape samples and can be considered as a follow up from our previous investigation, we propose the development of an EE sensing system for the prediction of colour-related parameters, principally suitable to monitor the phenolic maturity.

To this aim, purple grape samples were collected at different harvest times from veraison to maturity, then a drop of the derived must was deposited on a paper sheet to obtain a sort of paper chromatography. The spots of must were imaged by means of a flatbed scanner, and the resulting RGB images were analysed using multivariate methods, in order to use the colour-related information content of the images to predict the phenolic composition of the samples, and therefore to follow the phenolic ripening trend.

To date, few research studies reported the use of image analysis for the evaluation of colour characteristics and colour changes of grape berries during ripening. For instance, in [17, 18] RGB images of grape berries have been categorised into different classes according to ripening. More in detail, considering the histograms of colour-related parameters such as hue or brightness, proper threshold values have been identified to distinguish grapes into different clusters according to their colour development (e.g., pre-veraison and post-veraison). In other research papers, the digital images of grape seeds have been used to investigate CIELAB parameters and morphological features, such as area, aspect, roundness, length, width and heterogeneity, in order to predict their maturity stage [19, 20]. Notwithstanding the satisfactory results obtained in these studies, the proposed methods were limited to the identification of correlations between colour and/or morphological features and the maturity level of grapes, which was determined based on harvest time or on visual inspection by expert assessors.

In the present work, we followed an alternative approach based on the use of RGB images for the quantitative prediction of specific analytical parameters related to the colour properties and the phenolic composition of the grape samples, which could allow to obtain a more detailed and comprehensive overview of the maturity level.

Basically, our method consists in converting each image into a one-dimensional signal, named *colourgram*, which codifies all the colour-related information and represents a sort of fingerprint of the corresponding RGB image [21]. The main advantage of this approach is that the whole dataset of colourgrams can be analysed in the same manner as any other dataset of signals. For instance, exploratory analysis tools like Principal Component Analysis (PCA) can be used to highlight the presence of trends, of clusters or of outlier images, whereas multivariate calibration or classification methods can be used to predict the value of specific parameters or to assign a sample to a specific class, based on its colour-related characteristics.

The colourgram approach has been successfully applied for the automated solution of several colour-related issues concerning food industry, among which the quantification of defective maize kernels, related to the presence of mycotoxins [22], the detection of red skin defect of raw hams [23], the quantification of *Lactobacillus* in fermented milk [24], the prediction of the compositional and sensory characteristics of pesto sauce [25] and the classification of different pesto brands [21].

In this study, after an exploratory analysis of the colourgrams matrix by PCA, multivariate calibration models were developed using a feature selection/calibration algorithm, namely interval-Partial Least Squares (iPLS) [26]. The purpose was to define the correlation between the images of must spots and a series of twelve parameters related to the phenolic composition of the samples.

The use of iPLS was particularly profitable for identifying the colourgram features related to the changes in colour and phenolic composition of must samples during the grape berries ripening. Moreover, by using a proper algorithm [23] the selected features were displayed in the original image domain, allowing to evaluate the relevant colour features automatically selected by iPLS.

2 Materials and methods

2.1 Samples

In this study, three Italian purple grape varieties were considered: *Ancellotta* (A), *Lambrusco Marani* (L) and *Malbo Gentile* (M). The samples were collected in Reggio Emilia (Italy) during vintage 2015.

For each variety, grape sampling was conducted on three grapevines (field replicates) in order to account for the vineyard variability. More in detail, about 100 individual grape berries per grapevine were randomly gathered for each one of 5 subsequent harvest times (T0, T1, T2, T3, T4) at about 10-day intervals, starting from veraison and ending at harvest of the mature grapes. Therefore, 45 grape samples were collected on the whole, resulting from (3 grape varieties × 3 field replicates × 5 harvest times) and were immediately carried to the laboratory under refrigerated conditions. Each grape sample was crushed into a falcon tube under nitrogen atmosphere to prevent the oxidation of phenolic compounds. The crushed berries were left to macerate for 60 minutes at 4°C in the dark, then centrifugation at 4000 rpm for 15 minutes was performed (refrigerated centrifuge 4237R, ALC, Cologno Monzese, MI). The supernatant –called "must" from here onwards– was divided into two different aliquots to perform replicate determinations.

Each aliquot was stored at -20 °C and unfrozen just before spectrophotometric and chromatographic analyses, that were performed in parallel with image acquisition. All the analyses were replicated twice for each must sample: in the first measurement session the acquisition order was randomized, and the first aliquot of each sample was analysed. Then, the order was shuffled again and the second aliquot of each sample was analysed. The overall number of analyses was therefore equal to 90 (3 grape varieties × 5 harvest times × 3 field replicates × 2 analytical replicates).

2.2 Determination of parameters related to phenolic ripeness

The following twelve parameters were measured by means of spectrophotometric and chromatographic assays:

- total flavonoids content (TF) was determined by UV spectroscopy as reported in the literature [27]: after a proper dilution, the absorbance of the sample was measured at 280 nm and TF was expressed as mg of (+) catechin/L. All the UV-Vis measurements were

performed by means of a Perkin Elmer Lambda 650 spectrophotometer using a 10 mm quartz cuvette as sample holder. Before spectrophotometric analysis the samples were diluted 50 times in hydrochloric acid-ethanol solution (ethanol:H2O:HCl 70:30:1 v/v/v);

- total anthocyanins content (TAnt) was determined by UV-Vis spectroscopy according to the method described in [28]: the absorbance value was measured at 540 nm and TAnt was expressed as mg of oenin chloride/L;
- colour index (CI) was calculated as the sum of the absorbance values measured at 420 nm (corresponding to a yellow-orange sample colour), at 520 nm (corresponding to a red-purple sample colour) and at 620 nm (corresponding to a blue sample colour) [29]. In oenology, CI is used to evaluate the colour of red wines: if a wine needs a colour correction it is blended with a different wine up to the desired CI value;
- optical density values (OD420%, OD520%, OD620%) defined as the percentage contribution of each absorbance, at 420, 520 and 620 nm, to the colour index [30];
- tonality (Ton) was calculated as the ratio between the absorbance values measured at 420 nm and at 520 nm. In oenology, Ton is a parameter frequently used to assess the oxidation of wine during aging [30]. In this case, Ton is used as a parameter suitable to describe the colour variation which occurs during grape ripening;
- the five major anthocyanins in the form of 3-O-monoglucoside, i.e. malvidin (Mv-3-glc), petunidin (Pt-3-glc), peonidin (Pn-3-glc), delphinidin (Df-3-glc) and cyanidin (Cn-3-glc), were separated and quantified by reverse phase-high performance liquid chromatography with a diode array detector (RP-HPLC-DAD) following the chromatographic method described in [31] and adjusted to our equipment, as reported by Vasile Simone and co-authors [32]. The concentration of the anthocyanins was determined by measuring the absorbance at 520 nm by Total-Chrom Workstation version 6.2.1 chromatography system software (PerkinElmer, Inc.), and was expressed as malvidin-3-O-glucoside equivalents.

2.3 Image acquisition

From each aliquot of must sample obtained as described in Section 2.1, 50 µl drops of must were deposited on A4-sized sheets of white absorbent paper. For the deposition of the must drops, a precise scheme was used: 8 drops of each must sample were put on each sheet of absorbent paper following a 4×4 chessboard scheme, alternated to 8 drops of another randomly chosen sample. Therefore, each absorbent paper sheet contained 16 spots of two samples, i.e., 8 spots per sample (as an example, *see* the image on the left side of Figure 1).

Several paper types were tested to choose the most proper one to be used as a substratum for spot deposition. Among them, it was found that the absorbent and coated paper (weight: 120 g/m^2, thickness: 0.24 mm) gave more homogeneous spots due to the presence of two layers: an upper one, made of cellulose with a high liquid absorption capability, and a lower one, made of polyethylene with a high water resistance that allowed to prevent paper wrinkling.

RGB images of the paper sheets were acquired immediately after drops deposition using a CanoScan Lide 220 scanner and saved in JPEG format with a spatial resolution of 4960 × 7015 pixels and an average file size equal to 2 MB. The image scene included also a set of standard colour references used for the subsequent image standardization.

2.4 Image elaboration

The key steps followed for the elaboration of the RGB images are illustrated in the right side of Figure 1 and can be summarized as follows:

2.4.1 Internal calibration

The RGB images were firstly standardized by means of an internal calibration procedure, in order to reduce possible variability among images over time, mainly due to instrumental instability. The correction procedure reported here is derived from the approach already developed by some of us for the elaboration of hyperspectral images [33]. For each image, eight coloured squares of the standard colour references were considered as regions of interest (ROIs), and a random sampling procedure was used to divide the pixels of each ROI into three groups, in order to account for possible spatial variability of the coloured squares. For each pixel group, the corresponding median values of the R, G and B channels were calculated, then they were stored in a matrix with size equal to {24, 3}, i.e., including the 24 median values (= 3 pixel groups × 8 ROIs) for each one of the 3 channels.

The internal calibration step was carried out by computing, for each channel *c*, a regression model between the median vector extracted from the first acquired image, that was considered as the master image (*M*), and the median vector of each one of the remainder "slave" images (*S*). To select the most appropriate order of the regression model, the values of the first- and second-order regression coefficients were estimated, together with the corresponding statistical significances. Based on the results, for each slave image the quadratic models were finally considered, which can be expressed as:

$$M(c) = b_0(i, c) + b_1(i, c) \times S_i(c) + b_2(i, c) \times S_i^2(c) \qquad (1)$$

where b_0, b_1 and b_2 are the regression coefficients calculated for the channel c of the i-th slave image, S_i.

Then, the regression coefficients calculated using the standard colour references were used to standardize each pixel of the corresponding image of the must spots, according to the equation:

$$img_{corr}(i, c) = b_0(i, c) + b_1(i, c) \times img_{orig}(i, c) + b_2(i, c) \times [img_{orig}(i, c)]^2 \qquad (2)$$

where $img_{corr}(i, c)$ is the channel c of the i-th standardized image, $img_{orig}(i, c)$ is the corresponding channel of the original image, and $b_0(i, c)$, $b_1(i, c)$, $b_2(i, c)$ are the regression coefficients calculated by equation 1.

2.4.2 Cropping

After internal calibration, for each image each spot of must deposited on the paper was separately cropped to recover an image of size equal to 900 × 900 pixels. The cropping procedure generated a dataset of 720 images (= 3 grape varieties × 3 field replicates × 5 harvest times × 8 spots × 2 measurement sessions).

2.4.3 Spot segmentation

Before converting all the images into the corresponding colourgrams, a preliminary inspection of the frequency distribution curves of the parameters included in the colourgram was conducted on a representative subset of images. This inspection evidenced that the pixels with values of relative red (rR, *see* paragraph 2.4.4 for definition) lower than 0.34 correspond to the background (white paper sheet). Therefore, the colourgram of each image was calculated after background removal (segmentation), i.e., considering only the pixels of the spots which present rR values greater than 0.34.

2.4.4 Conversion into colourgrams

After spot segmentation, the images of the individual spots were converted into the corresponding colourgrams, following the procedure reported in [21].

Basically, the first step of this approach consists in unfolding each RGB image in a two-dimensional matrix with as many rows as the number of segmented pixels, and 3 columns, corresponding to the R, G and B channels. For each pixel, a series of additional variables directly derived by the R, G and B values are calculated: lightness (L), defined as the sum of R, G and B values; relative colours (rR, rG and rB), which are respectively the ratios between each channel and L; hue (H), saturation (S) and intensity (I), obtained by converting the RGB data into the HSI colour space, and the nine score vectors (three for each model) obtained by applying PCA to the raw,

meancentered and autoscaled unfolded image data. For each variable, the frequency distribution curve (i.e., a histogram with 256 bins) is calculated, then the histograms of the 19 variables are joined in sequence to form a unique one-dimensional signal, which is then divided by the number of segmented pixels. In the end, the loading vectors and the eigenvalues of the three PCA models are added to the signal, that reaches a final length equal to 4900 points (= 256 × 19 + 36).

The conversion of the image into a one-dimensional signal is useful to gain a considerable data compression, which results in a faster computation time necessary for data elaboration. Indeed, the obtained matrix of these fingerprint-like signals can be analyzed by means of common multivariate analysis techniques, such as PCA or PLS.

On the other hand, the colourgram does not account for the spatial location in the original image domain of the colour-related information extracted by multivariate analysis. To address this issue, a proper algorithm has been implemented to visualize directly in the original image domain the colourgram features of interest for the problem at hand. In other words, it is possible to have a reconstructed image where the pixels related to the colourgram features recognized as interesting by the user are displayed in false colours, while the remainder pixels are represented in black [23].

All the steps followed for image elaboration were performed with routines written *ad hoc* in MATLAB language (ver. 7.12, The Mathworks Inc., USA). In particular, the correction of the images and the subsequent conversion into colourgrams have been performed with specific Graphical User Interfaces (GUI): *RGB Image Correction GUI* and *Colourgrams GUI*, which are available at www.chimslab.unimore.it.

2.5 Multivariate analysis of colourgrams

PCA was firstly applied to the meancentered colourgrams matrix as an exploratory data analysis tool suitable to recognize similarities and differences among the images of must spots, also highlighting the possible presence of outliers.

Then, multivariate calibration models were calculated on the meancentered colourgrams matrix to quantitatively determine the values of the twelve considered parameters (Y variables). To this aim, the 720 colourgrams were split into a training set, used to calculate the models, and a test set, used for validation. In order to avoid overfitting, the splitting was conducted in a way to maintain together the colourgrams derived from replicate images: 480 colourgrams corresponding to 60 samples belonging to two field replicates were included in the training set, and the remainder 240 colourgrams corresponding to 30 samples belonging to the remaining field replicate were included in the test set.

The optimal number of Latent Variables (LVs) used to build each model was chosen by minimizing the Root Mean Square Error in Cross-Validation (RMSECV). A venetian-blinds cross-validation was performed considering 2 deletion groups, each one containing the signals corresponding to one field replicate.

The information brought by the different "peaks" (i.e., the frequency distribution curves) of the colourgram is partially redundant, since all those variables are derived from the RGB values of the pixels in the original image. Therefore, the selection of the most relevant descriptors from such a wide number of features could be useful to improve the performance of the calibration models and to reduce the time needed for image analysis in the perspective of an industrial application. Therefore, interval-PLS (iPLS) in the *forward* mode was used as a variable selection/calibration method on the meancentered colourgram matrix [26]. Basically, *forward* iPLS is an algorithm conceived to divide the signal into a certain number of intervals of equal width defined by the user. By iteratively adding one interval at a time, the algorithm selects the most effective intervals for calibration as the ones that, when added, produce a significant decrease of RMSECV. In this work, 6 iPLS models for each Y variable were calculated considering different interval widths, corresponding to 256, 128, 64, 32, 16 and 8 variables.

The performance of the calibration models are reported in terms of the Root Mean Square Error in calibration (RMSEC), in cross-validation (RMSECV), and in prediction (RMSEP), together with the coefficient of determination in calibration (R^2_{Cal}), in cross-validation (R^2_{CV}), and in prediction (R^2_{Pred}). The RMSE and R^2 values were calculated using the equations reported in [16].

The PCA, PLS and iPLS models were calculated using the PLS Toolbox (ver 8.1.1, Eigenvector Research Inc., USA) running in the MATLAB environment (ver. 7.12, The Mathworks Inc., USA).

3 Results and discussion

3.1 Exploratory data analysis

The PCA model calculated on the colourgrams matrix highlighted a trend according to harvest time that was clearly visible along the PC1 scores, as reported in Figure 2a. In general, it can be observed that PC1 values generally increase for the different grape varieties according to the harvest time. However, considering the single grape varieties, it is possible to recognise some minor clusters formed by samples picked in different time periods. The comparison of the PC1 score distribution with sample images collected at the five harvest times (Figure 2b), highlights that actually the observed clustering involves groups of spots having similar colour-related characteristics, i.e., that

there is a separation between spots having a lighter colour and spots having a more intense colour. For instance, the colourgrams derived from *Ancellotta* samples gather in two clusters, the first one composed of the light colour samples collected at T0 and T1, and the second one composed of the darker colour samples collected at T2, T3 and T4.

Moreover, the colour evolution of the must spots during grape ripening is different for the distinct varieties.

3.2 interval-PLS calibration models

For each Y variable 6 iPLS models were calculated considering different interval widths. Table 1 reports the results of the best calibration models selected in cross-validation, considering the lowest RMSECV value.

The overall best calibration model was obtained for the total amount of anthocyanins (R^2_{pred} = 0.94). This model has been built using only 416 variables (26 intervals made of 16 variables) out of 4900 original variables. The selected regions include variables belonging to several distribution curves of the colourgram, i.e., R, G, B, L, Rr, S, V, the score vectors of PC1-raw, PC3-raw, PC1-meancentred, PC1-autoscaled and PC2-autoscaled. The actual values versus the predicted values of TAnt for the test set samples are reported in Figure 3a.

The performance of the calibration model obtained for the prediction of TF were less good, even though acceptable (R^2_{pred} = 0.67). As a matter of fact, flavonoids are a large family of hydroxylated polyphenolic compounds: the major group consists of anthocyanins (red-purple pigments), but many other compounds belonging to the family of flavonoids are weakly coloured or colourless, such as flavonols (pale yellow pigments) and flavanols (colourless pigments that become brown in case of oxidation) [34]. Therefore, RGB images are more suitable to accurately predict the anthocyanins content, which increases during the maturation, strongly influencing the red-purple grape colour and, consequently, the colour of the resulting must.

Colour index is the most useful attribute to evaluate the overall colour of this kind of samples. For CI, a high predictive performance (R^2_{pred} = 0.91) was obtained considering only 576 variables, that were selected using an interval width of 32 variables. The most part of the selected regions belong to the same frequency distribution curves selected for the calibration of TAnt. In this case, variables from the histograms of R, G, B, L, H, S, V, score vectors of PC1-raw, PC3-raw, PC1-meancentred, PC2-meancentred, PC1-autoscaled and PC2-autoscaled were selected. This fact indicates that few regions of the colourgram are sufficient to have an accurate prediction of both TAnt and CI, which are among the most important parameters to monitor the phenolic ripening of grapes.

Satisfactory models were also obtained for the prediction of Ton (R^2_{pred} = 0.88), OD420% (R^2_{pred} = 0.91) and OD520% (R^2_{pred} = 0.86), whereas the estimate of OD620% was not even remotely possible. As it was already observed in [16], where analogous results were obtained for the prediction of this parameter also using the ET, this is likely due to the very low absorbance values measured at 620 nm, close to the baseline.

Concerning the calibration models of the single anthocyanins, the best result was obtained for the prediction of malvidin (Mv-3-glc, R^2_{pred} = 0.85), which is the most abundant anthocyanin in the considered grape varieties, and consequently the most responsible one for the red-purple colour of the corresponding must. Similar results were obtained for the prediction of petunidin (Pt-3-glc, R^2_{pred} = 0.84) and peonidin (Pn-3-glc, R^2_{pred} = 0.73). On the contrary, the calibration models for the prediction of delphinidin (Df-3-glc, R^2_{pred} = 0.59) and cyanidin (Cn-3-glc, R^2_{pred} = 0.09) showed a poor correlation between the amount of these anthocyanins and the colour variation of the images of must during the grape ripening.

Finally, it must be underlined that in this study the calibration models were calculated considering as separate items the eight colourgrams corresponding to the images of the eight spots obtained for each aliquot of must sample. In this manner, it was possible to evaluate the repeatability of the procedure through the estimate of the within-sample variability [22], i.e., of the variability of the spots of the same must sample. However, for an application on a real case scenario, the estimates of the parameters would be obtained as the average of the values predicted from images of multiple spots of the same sample. As an example, considering the best calibration model obtained for TAnt, Figure 3a reports the predictions for the single spots of the test set samples, while Figure 3b shows the corresponding average values.

Therefore, for completeness, Table 1 also reports the values of aRMSEP and aR^2_{Pred}, which correspond to the RMSEP and R^2_{Pred} values calculated considering the average of the eight *y* values estimated from the eight spots of each sample. As one might expect, the predictive performance of the calibration models obtained after averaging the results are improved.

3.3 Spatial interpretation of the results by means of images reconstruction

When using PLS-based algorithms for calibration or classification purposes, it is a common practice to look at the Variable Importance in Projection (VIP) plots to identify the most relevant variables. Indeed, the variables having VIP scores higher than a threshold value, generally set to 1, are considered significant for the model [35]. The comparison of the VIP scores of the iPLS models calculated for the prediction of TAnt, CI and Mv-3-glc (Figure 4) shows that the most important

colourgram region is the same for the three models, and corresponds to the score vector of PC3 obtained by applying PCA to the raw unfolded RGB matrix (SC3RAW).

In order to interpret the results of the models, the original images were reconstructed by considering only the pixels falling in the selected interval of SC3RAW. Figure 5 reports the reconstruction of five images for each grape variety at the different maturity levels, from T0 to T4, together with the corresponding original segmented images. It is possible to notice a common trend regardless of the grape variety. In fact, the number of reconstructed pixels increases in accordance with the degree of grape maturity: at T0 only few pixels belonging to the must spot appear in the reconstructed image, while at T4 most of the spot pixels of the original image are present in the corresponding reconstructed image. Therefore, the informative colour-related parameters, identified by means of a blind approach, correspond to the pixels related to high values of both colour index and total anthocyanins content, that is mainly due to malvidin-3-O-glucoside.

A final remark concerns the time needed for computation: the conversion of one image into the corresponding colourgram and the prediction of the considered parameters require only few seconds, and the whole procedure can be easily automated. Conversely, the determination of the same parameters related to grape ripening by means of classical analytical methods would require much longer times.

4 Conclusions

In the present paper we investigated the possibility of using an electronic eye, consisting of a common flatbed scanner, to monitor the phenolic ripening of grapes. This electronic eye allowed to obtain acceptable to satisfactory predictions for nine out of twelve parameters related to phenolic ripening, based on multivariate analysis of the images of grape musts spots.

The most interesting outcome is that these results are complementary to those obtained on the same samples using an ET sensing system [16]: indeed, the EE is suitable to predict parameters related to the phenolic ripeness (anthocyanins), while the ET is suitable to predict parameters related to the technological ripeness (sugars and acidity). Therefore, the original idea behind these studies becomes realistic: to develop a fast, inexpensive and eco-friendly method, based on a combined device, which is able to easily quantify the parameters related to technological and phenolic maturity. To this aim, further investigations are being conducted to condense the information brought by EE and ET through the use of different data fusion strategies.

More in general, the EE-based analytical system developed in the frame of the present study could be easily adapted for the quantitative and/or qualitative assessment of colour-related properties of liquid samples. Indeed, the proposed approach could be extended to all those situations in which the

colour of a solution is strictly related to the presence of one or more analytes of interest. Therefore, further applications could be not necessarily limited to the food industry, e.g. for the analysis of other beverages like wine, fruit juice, beer and coffee, but also in other contexts; for example, after proper adjustments, this approach could be also helpful for the analysis of specimens of forensic or clinical interest, among others.

Conflict of interest

The authors declare that they have no conflict of interest.

Acknowledgements

The authors acknowledge financial support for this research by University of Modena and Reggio Emilia through FAR 2014. The Authors are grateful to "Istituto Superiore A. Zanelli", Reggio Emilia – Italy, for providing grape samples.

References

[1] A.A. Kader, Fruit maturity, ripening, and quality relationships, Acta Hortic. 485 (1999) 203–208.

[2] D.I. Jackson, P.B. Lombard, Environmental and Management Practices Affecting Grape Composition and Wine Quality - A Review, Amer. J. Enol. Viticult. 44 (1993) 409–430.

[3] R. Gawel, Red wine astringency: a review, Austr. J. Grape Wine R. 4(2) (1998) 74–95.

[4] E. Obreque-Sliera, A. Peña-Neiraa, R. López-Solísb, A. Cáceres-Mellaa, H. Toledo-Arayab, A. López-Riverab, Phenolic composition of skins from four Carmenet grape varieties (Vitis vinifera L.) during ripening, LWT - Food Sci. Tech. 54(2) (2013) 404–413.

[5] E. Ferrari, G. Foca, M. Vignali, L. Tassi, A. Ulrici, Adulteration of the anthocyanin content of red wines: Perspectives for authentication by Fourier Transform-Near InfraRed and 1H NMR spectroscopies, Anal. Chim. Acta 701(2) (2011) 139–151.

[6] R. Ferrer-Gallego, J.M. Hernández-Hierro, J.C. Rivas-Gonzalo, T.M. Rivas-Gonzalo, Determination of phenolic compounds of grape skins during ripening by NIR spectroscopy, LWT – Food Sci. Tech. 44(4) (2011) 847–853.

[7] M. Le Moigne, C. Maury, D. Bertrand, F. Jourjon, Sensory and instrumental characterisation of Cabernet Franc grapes according to ripening stages and growing location, Food Qual. Pref. 19(2) (2008) 220–231.

[8] J.M. Murraya, C.M. Delahuntyb, I.A. Baxtera, Descriptive sensory analysis: past, present and future, Food Res. Int. 34(6) (2001) 461–471.

[9] M. Śliwińska, P. Wiśniewska, T. Dymerski, J. Namieśnik, W. Wardencki, Food Analysis using artificial senses, J Agric Food Chem. 62(7) (2014) 1423-48.

[10] A. Loutfi, S. Coradeschi, G.K. Mani, P. Shankar, J.B.B. Rayappan, Electronic noses for food quality: A review, J. Food Eng. 144 (2015) 103–111.

[11] J. Gutiérrez, M.C. Horrillo, Advances in artificial olfaction: Sensors and applications, Talanta 124 (2014) 95–105.

[12] Y. Tahara, K. Toko, Electronic tongues-a review, IEEE Sens. J. 13(8) (2013) 6516019, 3001–3011.

[13] L. Escuder-Gilabert, M. Peris, Review: Highlights in recent applications of electronic tongues in food analysis, Anal. Chim. Acta 665(1) (2010) 15–25.

[14] D. Wu, D.-W. Sun, Colour measurements by computer vision for food quality control - A review, Trends Food Sci. Tech. 29(1) (2013) 5–20.

[15] P. Jackman, D.-W. Sun, Recent advances in image processing using image texture features for food quality assessment, Trends Food Sci. Tech. 29(1) (2013) 35–43.

[16] L. Pigani, G. Vasile Simone, G. Foca, A. Ulrici, F. Masino, L. Cubillana-Aguilera, R. Calvini, R. Seeber, Prediction of parameters related to grape ripening by multivariate calibration of voltammetric signals acquired by an electronic tongue, Talanta 178 (2018) 178–187.

[17] Z. Pothen, S.T. Nuske, Automated assessment and mapping of grape quality through image based color analysis, IFAC-PapersOnLine. 49(16) (2016) 72–78.

[18] F.J. Rodrìguez-Pulido, L. Gòmez-Robledo, M. Melgosa, B. Gordillo, M.L. Gonzàlez-Miret, F.J. Heredia, Ripeness estimation of grape berries and seeds by image analysis, Comput. Electron. Agric. 82 (2012) 128–133.

[19] F. Avila, M. Mora, C. Fedres, A method to estimate grape phenolic maturity based on seed images, Comput. Electron. Agric. 101 (2014) 76–83.

[20] F.J. Rodrìguez-Pulido, R. Ferrer-Gallego, M.L. González-Miret, J.C. Rivas-Gonzalo, M.T. Escribano-Bailón, F.J. Heredia, Preliminary study to determine the phenolic maturity stage of grape seeds by computer vision, Anal. Chim. Acta 732 (2012) 78–82.
[21] A. Antonelli, M. Cocchi, P. Fava, G. Foca, G.C. Franchini, D. Manzini, Automated evaluation of food colour by means of multivariate image analysis coupled to a wavelet-based classification algorithm, Anal. Chim. Acta 515 (2004) 3–13.
[22] G. Orlandi, R. Calvini, G. Foca, A. Ulrici, Automated quantification of defective maize kernels by means of multivariate image analysis, Food Control 85 (2018) 259-268.
[23] A. Ulrici, G. Foca, M.C. Ielo, L.A. Volpelli, D.P. Lo Fiego, Automated identification and visualization of food defects using RGB imaging: Application to the detection of red skin defect of raw hams, Innov. Food Sci. Emerg. Tech. 16 (2012) 417–426.
[24] A. Borin, M. F. Ferrão, C. Mello, L. Cordi, L. C. Pataca, N. Durán, R. J. Poppi, Quantification of *Lactobacillus* in fermented milk by multivariate image analysis with least-squares support-vector machines. Anal. Bioanal. Chem., 387(3) (2007) 1105-1112.
[25] G. Foca, F. Masino, A. Antonelli, A. Ulrici, Prediction of compositional and sensory characteristics using RGB digital images and multivariate calibration techniques, Anal. Chim. Acta 706 (2011) 238–245.
[26] L. Norgaard, A. Saudland, J. Wagner, J.P. Nielsen, L. Munck, S.B. Engelsen, Interval partial least-squares regression (iPLS): a comparative chemometric study with an example from near-infrared spectroscopy, Appl. Spectrosc. 54(3) (2000) 413–419.
[27] R. Di Stefano, M.C. Cravero, N. Gentilini, Metodi per lo studio dei polifenoli dei vini L'Enotecnico XXV (5) (1989) 83–89.
[28] R. Di Stefano, M.C. Cravero, Metodi per lo studio dei polifenoli dell'uva Rivista di Viticoltura e di Enologia 2 (1991) 37–45.
[29] Y. Glories, La couleur des vins rouges. Mesure, origine et interprétation. Partie I, Connaiss. Vigne Vin. 18 (1984) 195–217.
[30] P. Ribéreau-Gayon, Y. Glories, A. Maujean, D. Dubourdieu, Handbook of Enology Volume 2: The Chemistry of Wine Stabilization and Treatments, John Wiley & Sons, New York, 2006, p. 178.
[31] F. Chinnici, F. Sonni, N. Natali, S. Galassi, C. Riponi, Colour features and pigment composition of Italian carbonic macerated red wines, Food Chem. 113(2) (2009) 651–657.
[32] G. Vasile Simone, G. Montevecchi, F. Masino, V. Matrella, S.A. Imazio, A. Antonelli, C. Bignami, Ampelographic and chemical characterization of Reggio Emilia and Modena (northern Italy) grapes for two traditional seasonings: ‘saba’ and ‘agresto’, J. Sci. Food Agric. 93 (2013) 3502–3511.
[33] A. Ulrici, S. Serranti, C. Ferrari, D. Cesare, G. Foca, G. Bonifazi, Efficient chemometric strategies for PET-PLA discrimination in recycling plants using hyperspectral imaging, Chemom. Intell. Lab. Syst. 122 (2013) 31–39.
[34] E. Petrussa, E. Braidot, M. Zancani, C. Peresson, A. Bertolini, S. Patui, A. Vianello, Plant flavonoids – biosynthesis, transport and involvement in stress responses, Int. J. Mol. Sci. 14(7) (2013) 14950–14973.
[35] G. Foca, D. Salvo, A. Cino, C. Ferrari, D.P. Lo Fiego, G. Minelli, A. Ulrici, Classification of pig fat samples from different subcutaneous layers by means of fast and non-destructive analytical techniques, Food Res. Int. 52 (2013) 185–197.

Captions to Tables and Figures

Table 1 – Results of the best iPLS calibration models obtained for the colour-related parameters.

Figure 1 – Acquisition scheme of the RGB images and key steps followed for the image elaboration.

Figure 2 – Sample index *vs.* PC1 score values (a); representative RGB images of Ancellotta, Lambrusco and Malbo Gentile must spots collected at the five harvest times (b).

Figure 3 – Actual amount of total anthocyanins (TAnt, expressed as mg of oenin chloride/L) *vs.* predicted amount, for the test set samples. Results obtained considering each single spot (a) and the averages over the eight spots (b).

Figure 4 –VIP scores plot resulting from the calibration models of TAnt, CI and Mv-3-glc. The zoom corresponds to the SC3RAW variables.

Figure 5 – Segmented RGB images and corresponding reconstructed images of five must spots at different maturity levels, for each grape variety.

Table1

Y variable	Interv. width	# of vars	# of LVs	RMSEC	RMSECV	RMSEP	aRMSEP	R^2_{Cal}	R^2_{CV}	R^2_{Pred}	aR^2_{Pred}
TF *	8	232	2	18.69	18.91	25.35	25.02	0.86	0.85	0.67	0.68
TAnt *	16	416	10	11.51	15.03	21.78	20.00	0.98	0.97	0.94	0.95
Ton	8	240	6	0.07	0.08	0.12	0.12	0.97	0.96	0.88	0.88
CI	32	576	8	0.57	0.72	1.05	0.99	0.97	0.95	0.91	0.92
OD420%	8	224	9	2.02	2.46	3.41	3.24	0.97	0.96	0.91	0.93
OD520%	8	184	8	3.12	3.26	4.62	4.55	0.95	0.94	0.86	0.86
OD620%	8	192	9	1.29	1.47	1.97	1.88	0.66	0.56	-1.50	-1.29
Df-3-glc *	8	200	8	2.24	2.29	8.69	8.65	0.91	0.90	0.59	0.59
Cn-3-glc *	8	272	8	1.33	1.48	6.86	6.83	0.85	0.81	0.09	0.10
Pt-3-glc *	8	296	8	3.76	3.54	5.92	5.84	0.91	0.92	0.84	0.84
Pn-3-glc *	8	184	9	5.08	5.93	8.37	8.05	0.81	0.74	0.73	0.75
Mv-3-glc *	8	248	8	16.37	19.10	29.04	27.88	0.96	0.95	0.85	0.86

** values in mg/L*

Figure1

Click here to download high resolution image

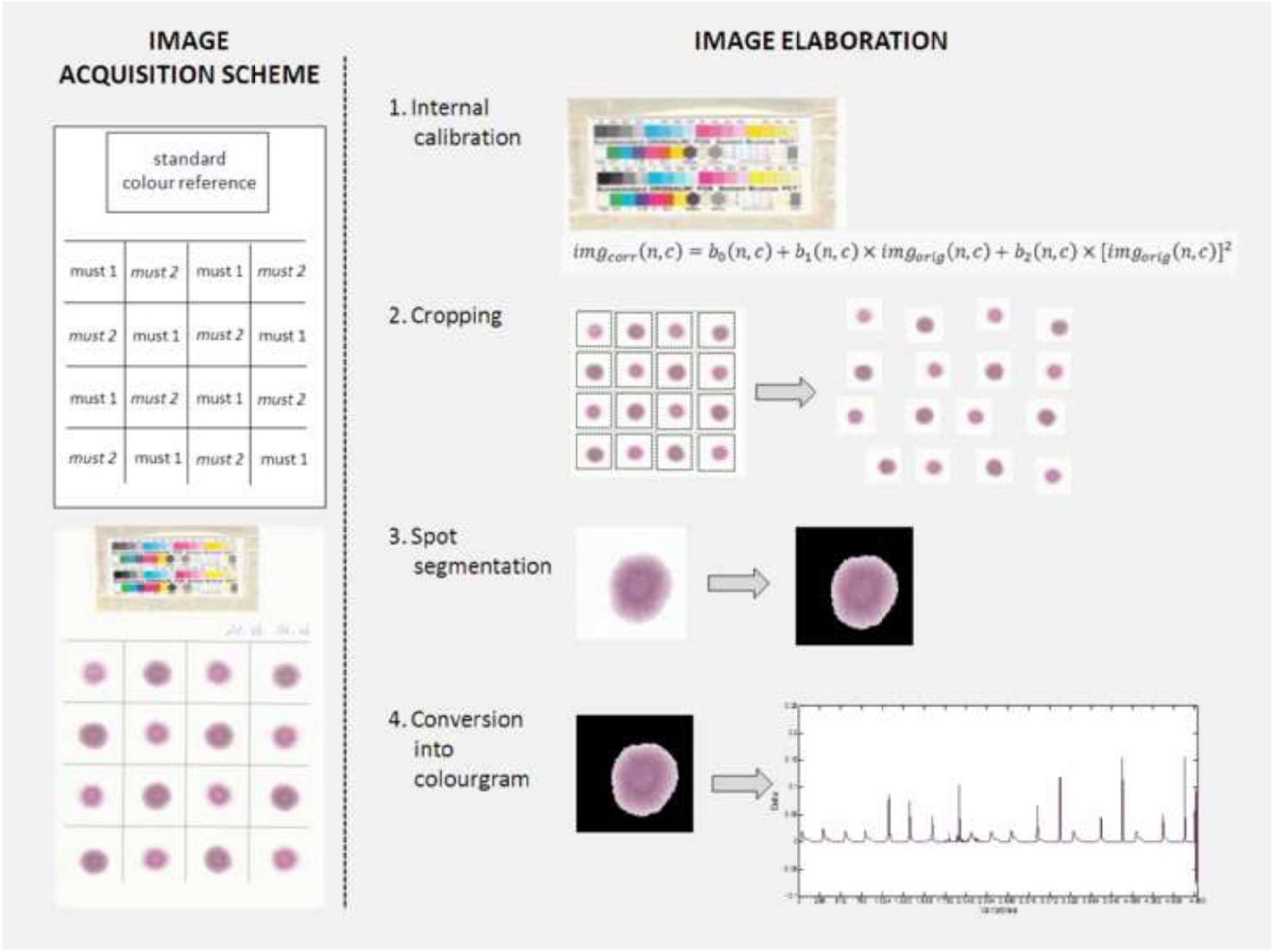

Figure2
Click here to download high resolution image

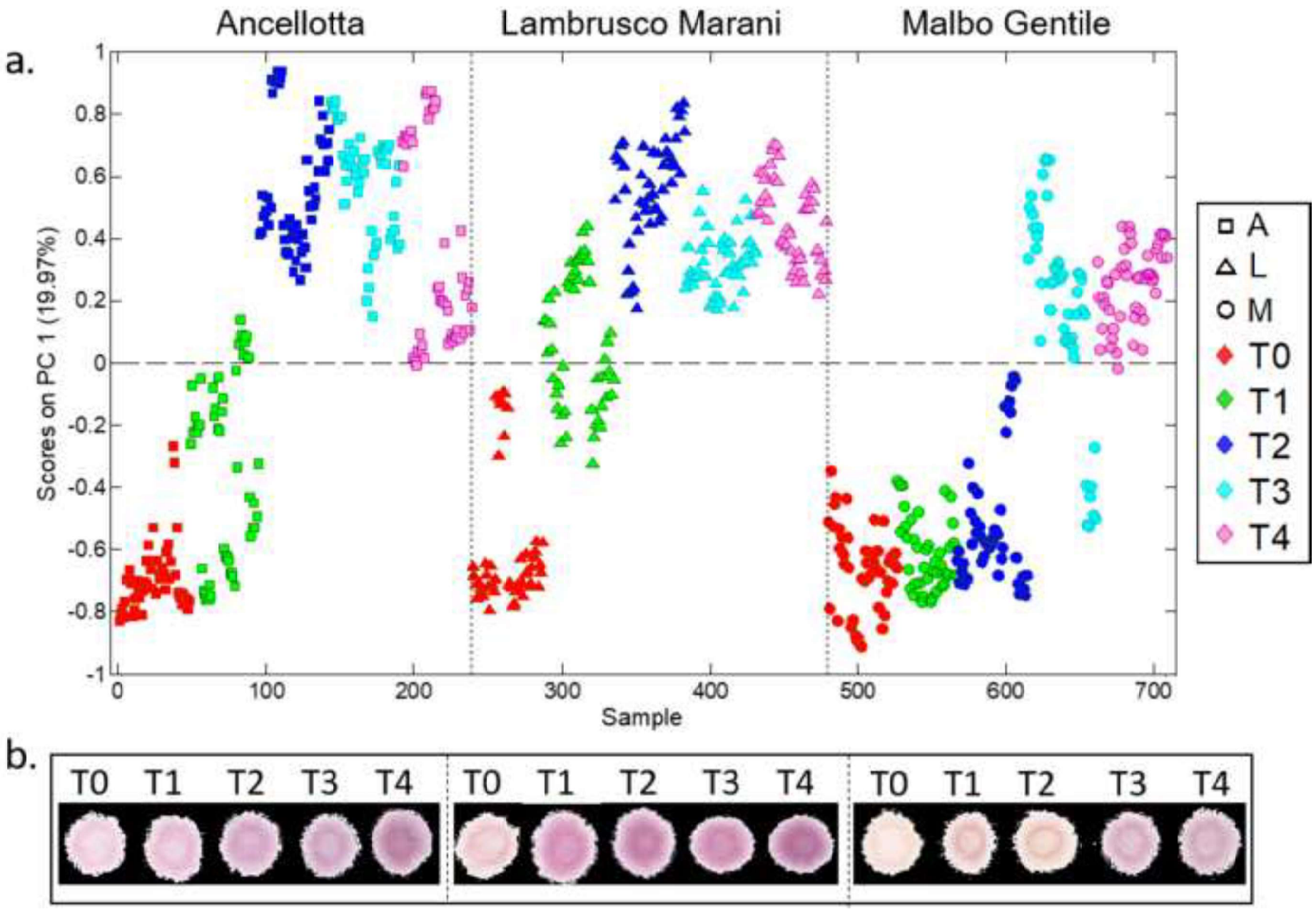

Figure3
Click here to download high resolution image

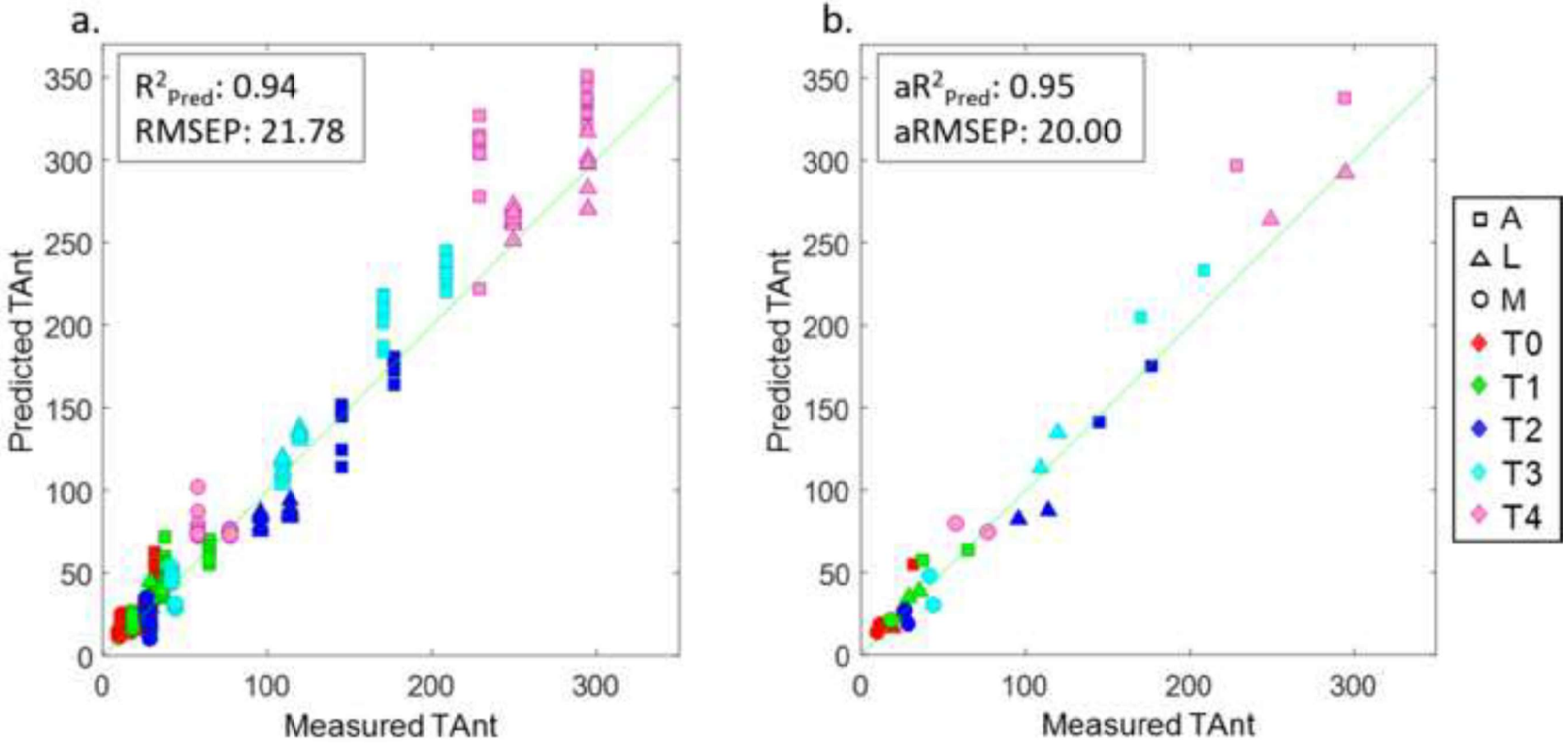

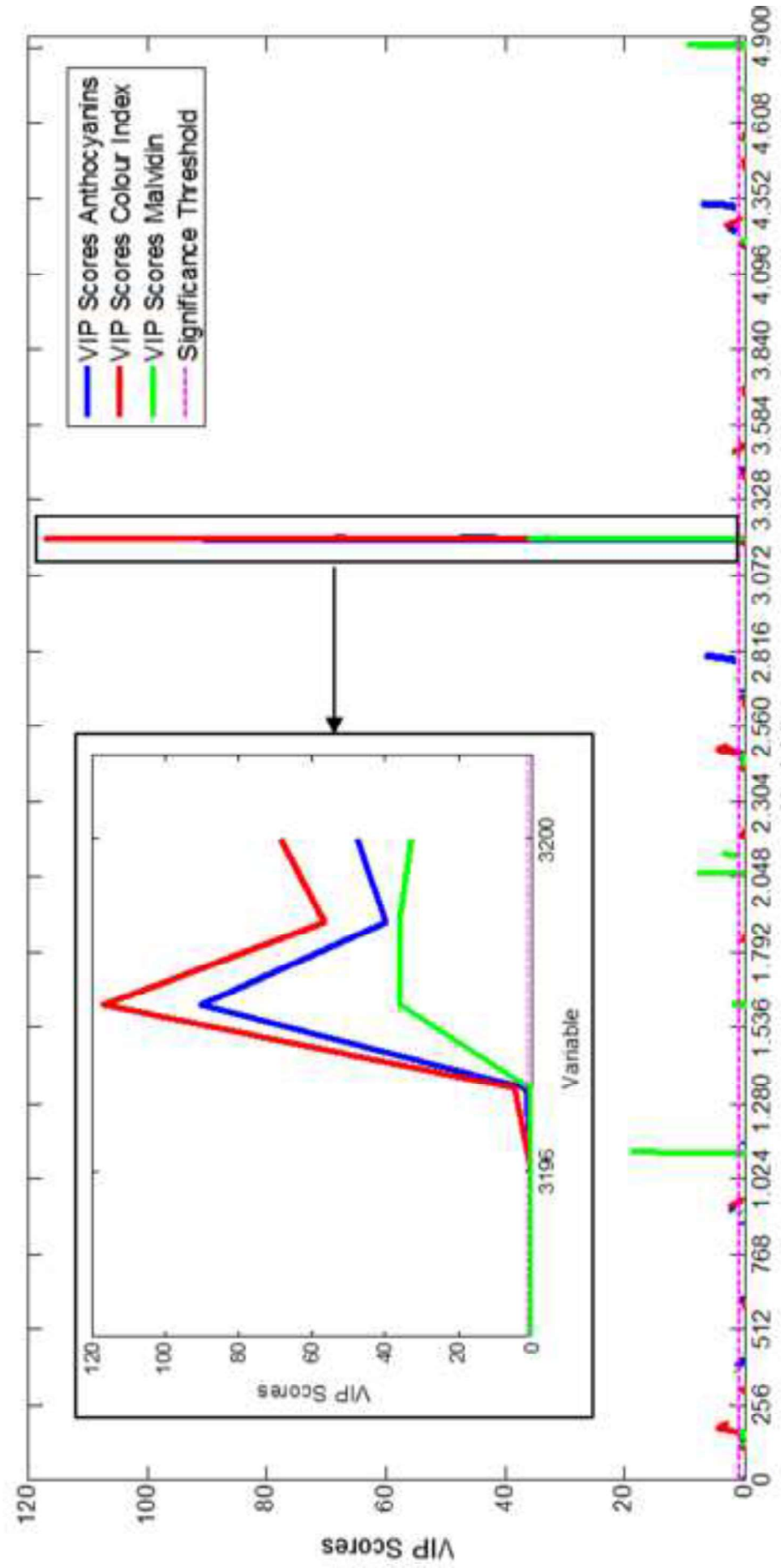

Figure4
Click here to download high resolution image

Figure5

Click here to download high resolution image

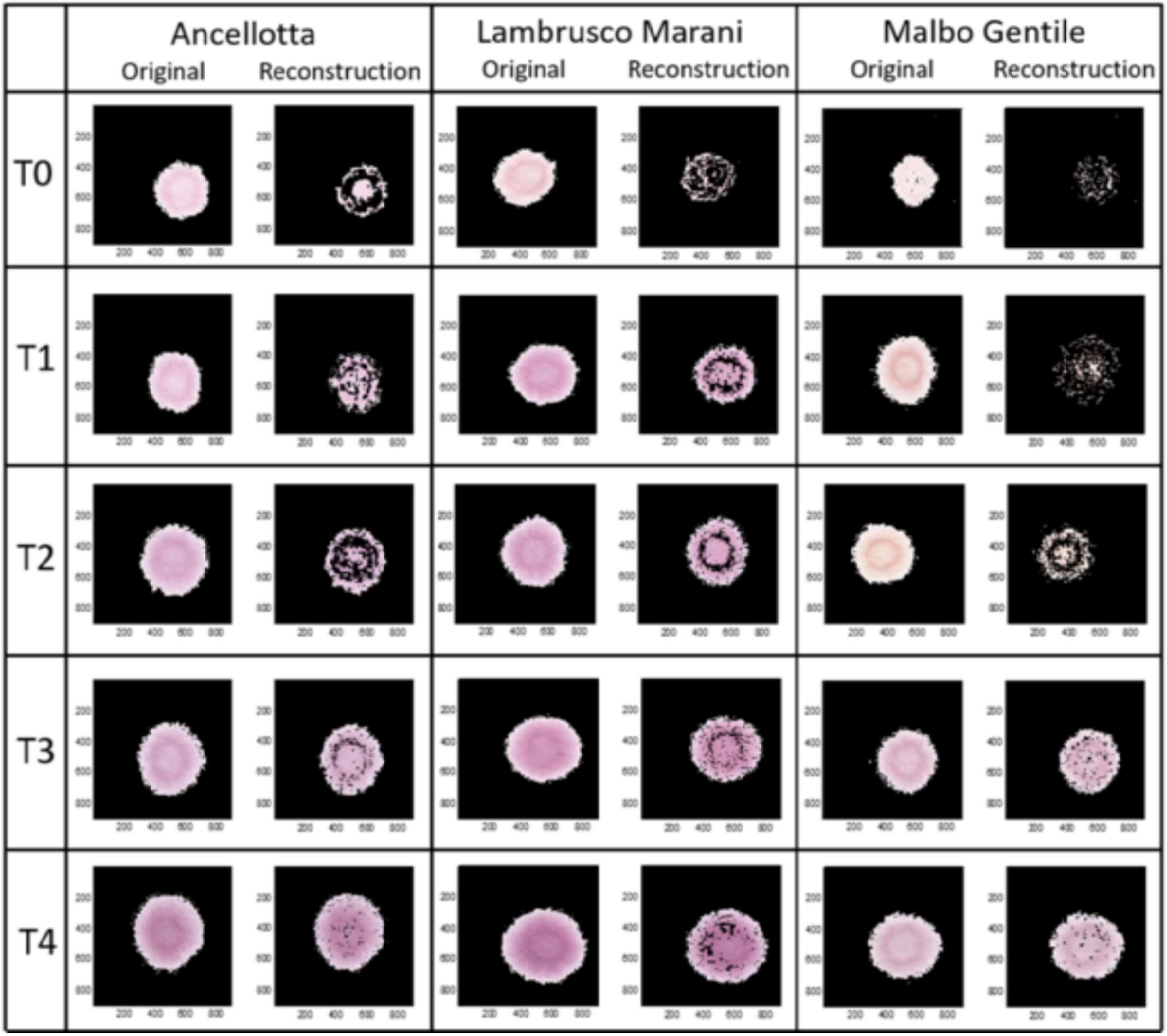

*Graphical Abstract (for review)

Click here to download high resolution image